**Summary:** A sample of poly(1-octadecene), synthesized with a highly active heterogeneous Ziegler-Natta catalyst, has been fractioned with heptane, giving soluble and insoluble fractions. Both fractions and the original polymer have been characterized by size exclusion chromatography, solution and solid-state $^{13}C$ NMR, DSC and X-ray diffraction. The results show that the fractionation occurs on the basis of both molecular mass and tacticity differences, with the atactic content concentrated in the lower molecular mass chains. Thus, the soluble fraction, having a lower average molecular mass than the original sample, consists predominantly of atactic chains, whereas the insoluble fraction is mainly isotactic. The analysis of the solid-state structure reveals that both atactic and isotactic fractions are able to crystallize, although their crystalline structures are different. The NMR and X-ray data together support the ''most probable'' structure for the isotactic polymer advanced by Turner-Jones. That structure is characterized by an orthorhombic crystal form, where a) the backbone crystallizes in a quaternary helical conformation, b) the sidechains are packed in a way analogous to orthorhombic polyethylene, and c) successive sidechains are conformationally inequivalent. Support for points b) and c) are respectively found in the chemical shift of the sidechains and in the splittings observed for backbone carbons and for some sidechain carbons located near the points of attachment. In addition, there is evidence that the mobility of sidechain sites at points near both the bonded and free ends are not uniform from chain to chain. On the other hand, the crystal form for the atactic polymer shows only sidechain order with some support for the notion that this order approximates the disordered hexagonal rotator phase of the alkanes.
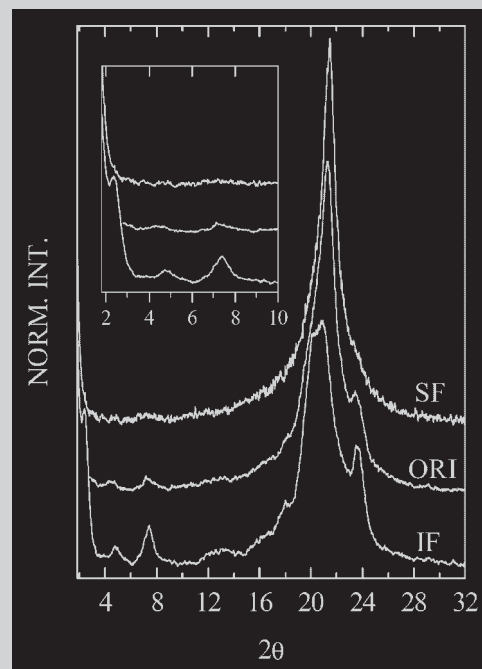
X-ray diffractograms of the three poly(1-octadecene) samples.

# Effect of Tacticity on the Structure of Poly(1-octadecene)

*David L. VanderHart,*[1] *Ernesto Pérez,*[2] *Antonio Bello,*[2] *Jaime Vasquez,*[3] *Raúl Quijada*[3]

[1] Polymers Division, National Institute of Standards and Technology, Gaithersburg MD 20899, USA
[2] Instituto de Ciencia y Tecnología de Polímeros (CSIC), Juan de la Cierva 3, 28006-Madrid, Spain
 E-mail: ernestop@ictp.csic.es
[3] Departamento de Ingeniería Química, Facultad de Ciencia Físicas y Matemáticas, Universidad de Chile y Centro para la Investigación Interdisciplinaria Avanzada en Ciencia de Materiales, Casilla 2777, Santiago, Chile

## Introduction

Long-chain poly(α-olefins) are a class of comblike polymers that present special properties due to the possibility of crystallization of the side branches when their length exceeds a certain number of carbons.[1−3]

One of the important characteristics of these polymers is the stereoregularity of the branches. This can be controlled by the appropriate choice of the catalyst system.[4−6] When heterogeneous Ziegler-Natta catalysts are used, the presence of two types of active centers with different stereospecificity leads to the formation of heterogeneous

polymers composed of varying amounts of atactic and isotactic chains. Owing to the differences in solubility of these two types of chains, it has been shown that they can be separated by solvent fractionation.[4,7−9]

The crystalline structure of isotactic poly(α-olefins) has been systematically studied by Turner-Jones,[10] finding three different crystal modifications in the long-chain types, depending on the thermal history imposed on the samples. He also postulated the most probable structures for each of these modifications. This polymorphic behavior is complicated by the fact that atactic chains, often coexisting in these comblike polymers, are also able to crystallize. Thus, the corresponding analysis of the crystalline structure of the atactic polymer should also be done.

The aim of this paper is to get further insight into the crystalline structure of poly(1-octadecene), POD, by analyzing the properties of samples with different tacticities.

## Experimental Part

The polymerization of 1-octadecene was carried out at 70 °C in a 250 ml glass reactor, in heptane solution, by using a highly active $MgCl_2$-supported $TiCl_4$ catalyst, activated by $AlEt_3$. The Al/Ti molar ratio in this catalyst was 150. The activity was found to be 400 kg polymer/h · g Ti. The crude polymer was isolated and purified. This original sample, designated "ORI", was fractionated by extraction with boiling heptane, giving a soluble and an insoluble fraction (abbreviated SF and IF, respectively).

Size exclusion chromatography, SEC, data were obtained using a Waters 150C gel permeation chromatograph, using different polystyrene standards as reference, and chloroform as eluent at 25 °C. From the peak maxima of the different chromatograms, the relative peak molecular masses, $\bar{M}_p^*$, were obtained. These values were then corrected for the nonlinearity of the chains.[11,12] The results for the corrected $\bar{M}_p$ are given in Table 1.

The thermal properties were measured by means of a Perkin Elmer DSC7 calorimeter, connected to a cooling system and calibrated with different standards. A scanning rate of 20 °C/min was used.

Solution-state $^{13}C$ nuclear magnetic resonance (NMR) spectra were acquired with a Varian spectrometer (at 75 MHz) using solutions of deuterated chloroform at 40 °C. A delay time of 2 s between pulses was used to assure the complete relaxation of the different carbon signals.[8,9]

Solid-state NMR experiments were conducted on a noncommercial, 2.35 T spectrometer operating at 25.2 MHz for $^{13}C$ nuclei. A noncommercial magic angle spinning (MAS) probe was utilized, which incorporated a MAS rotor/stator built by Doty Scientific of Columbia, SC. Spinning frequencies were 4 kHz. Cross-polarization (CP) was combined with MAS in the usual way[13] for acquiring CPMAS spectra. CP times varied from 0.7 to 1 ms. Fixing the CP time and varying the proton spin locking pulse length, prior to cross polarization enabled us to estimate rotating-frame relaxation times, $T_{1\rho}^H$, for the protons. Since the $T_{1\rho}^H$'s of protons in the crystalline (CR) and noncrystalline (NC) regions are usually different, linear combinations of spectra with different spin locking times were used, whenever possible, to extract the spectra associated with the CR and NC regions.[14] The method of Torchia[15] was also employed for estimating the longitudinal relaxation times, $T_1^C$, for individual carbons. Radio frequency field strengths corresponded to nutation frequencies of 69 and 65 kHz, respectively, for $^{13}C$ nuclei and protons. All spectra were recorded at ambient temperature (22 °C). Chemical shifts were measured, relative to liquid tetramethylsilane at 0 ppm, using the secondary standard, adamantane, as an external reference. The methine resonance of the latter is at 29.5 ppm.[16]

Wide-angle X-ray scattering (WAXS) patterns were recorded in the reflection mode at room temperature by using a Philips diffractometer with a Geiger counter, connected to a computer. Ni-filtered Cu Kα radiation was used. The diffraction scans were collected over a period of 20 min in the range of $2\theta$ values from 1.8 to 41.8°, using a sampling rate of 1 Hz. The goniometer was calibrated with a silicon standard.

Standard uncertainties given for the measured quantities represent estimates of two standard deviations.

## Results and Discussion

The DSC melting curves corresponding to the original polymer and the two fractions are shown in Figure 1. The original polymer possesses two main endotherms centered at 36 and 67 °C. However, the low temperature peak is dominant in the SF sample, whereas the high temperature one constitutes the major endotherm of the IF sample. Previous studies of different long-chain poly(α-olefins)[4,6,8,9] have shown that these low and high temperature endotherms are associated with predominantly atactic and isotactic chains, respectively. If this is true, the results in Figure 1 indicate that the solvent fractionation was not perfect, since a certain fraction of the SF sample melts at high temperature, whereas the IF fraction shows a minor peak at low temperature.

The solution-state $^{13}C$ NMR spectra of the three samples are shown in Figure 2. Some of the carbon signals in the spectrum of sample SF appear as multiplets and others are broader with varying resolutions, indicating a low degree of stereoregularity in this sample. However, sharper signals

Table 1. Peak molecular mass,[a] total enthalpy of melting[b] and isotactic content[c] of the poly(1-octadecene) samples.

| Sample | $\bar{M}_p \times 10^{-3}$ | $\Delta H_m^{total}$ | Isotactic content | |
|---|---|---|---|---|
| | g/mol | J/g | DSC | NMR |
| IF | 142 | 118 | 89 | 90 |
| ORI | 116 | 114 | 60 | 50 |
| SF | 43 | 108 | 19 | 20 |

[a] Standard uncertainty: ± 10% of values given.
[b] Standard uncertainty: ± 5 J/g.
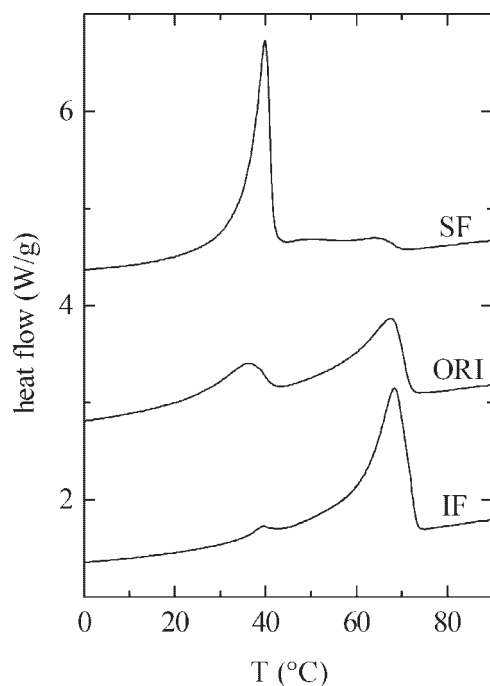[c] Standard uncertainty: ± 10% of values given.

Figure 1. DSC melting curves of the three poly(1-octadecene) (POD) samples. From top to bottom: soluble fraction (SF), orginal sample (ORI) and insoluble fraction (IF).

Table 2. Experimental and calculated chemical shifts for the $^{13}$C NMR spectrum of insoluble fraction (IF) sample.

| Carbon[a] | $\delta$ | |
| --- | --- | --- |
| | ppm | |
| | Experimental[b] | Calculated[c] |
| $\alpha$ | 40.34 | 39.48 |
| br | 32.48 | 32.91 |
| 16B | 35.04 | 34.97 |
| 15B | 26.63 | 27.51 |
| 14B | 30.40 | 30.21 |
| 13B | 29.42 | 29.96 |
| 12B–5B | 29.81, 29.83, 29.86, 29.89, 29.92 (2), 29.97 (2) | 29.96 |
| 4B | 29.74 | 29.71 |
| 3B | 31.98 | 32.4 |
| 2B | 22.70 | 22.65 |
| 1B | 14.06 | 13.86 |

[a] See Figure 3 for the designations.
[b] In CDCl$_3$ solution at 40 °C; standard uncertainty $= \pm 0.02$ ppm.
[c] According to ref.[18]

are obtained for the IF sample (the original sample exhibits signals in between the two fractions).

The assignments of the different carbons to the experimental chemical shifts for sample IF are presented in
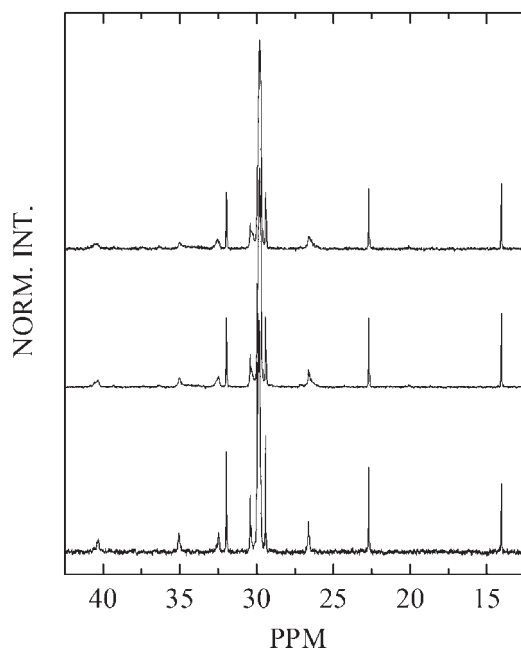
Table 2, where the nomenclature proposed by Randall[17] is followed, i.e., according to the scheme of Figure 3. Table 2 also shows the chemical shifts calculated by the method of Lindeman and Adams.[18] In general, a good agreement is found between the experimental and calculated values, although this semiempirical computational method predicts the same chemical shift for the nine central carbons in the branch. Considering that the width of the resonances is
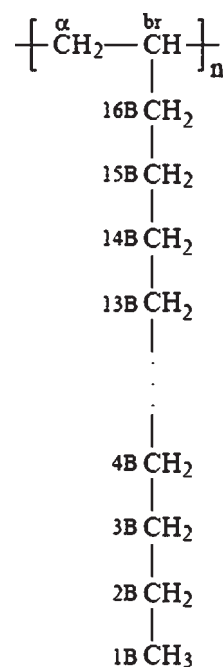


Figure 2. $^{13}$C NMR spectra of the three POD samples in solution of deuterated chloroform. From top to bottom: soluble fraction (SF), orginal sample (ORI) and insoluble fraction (IF) (for peak assignments: see Figure 3 and Table 2).



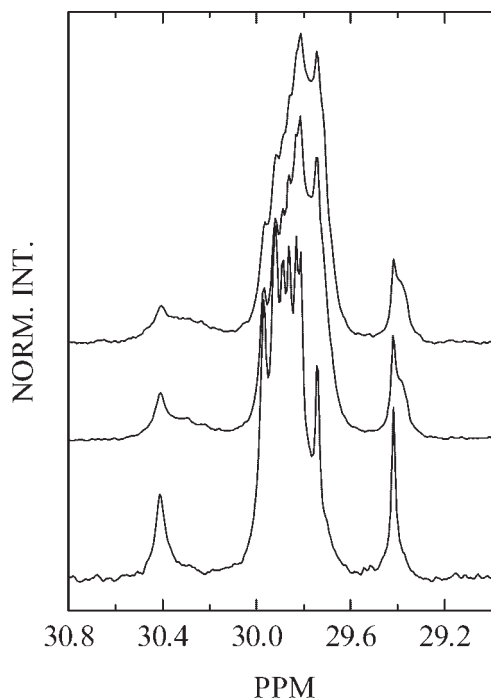Figure 3. Molecular formula of POD with the carbon designations.

Figure 4. Amplified region of the solution $^{13}$C NMR spectra of the three POD samples. From top to bottom: soluble fraction (SF), original sample (ORI) and insoluble fraction (IF) (for peak assignments: see Figure 3 and Table 2).

expected to be broader the closer the carbon is to the main chain, the peak appearing at 29.42 ppm has been assigned to carbon 13B. Moreover, in the expanded spectra of Figure 4, the IF sample shows six partially resolved resonances for the remaining unassigned eight central carbons, with the chemical shifts reported in Table 2. If resolution enhancement is applied to this spectrum, the deconvolution shows that the two downfield resonances of this group each contribute an area corresponding to two carbons. Moreover, it has to be considered that the present spectra have been acquired at relatively low temperature (40 °C, in chloroform). The resolution might be even better using a spectrometer of higher field or a solvent allowing higher temperatures of acquisition.

The expanded spectra in Figure 4 clearly show the tacticity effects mentioned above, especially for carbon 14B. For this resonance, the sharper signal at 30.40 ppm is most probably due to the *mmmm* pentad, so that the isotactic content can be estimated from its integration over the entire area of resonance, assuming that the Overhauser enhancement is similar for all the stereosequences. The corresponding results are listed in Table 1. Although the error involved in this determination is rather high, it is clear that the insoluble fraction is mostly isotactic, whereas a minor fraction of isotactic chains is present in the soluble fraction. This is in accordance with the DSC results in Figure 1, assuming that the low temperature peak arises from the

atactic chains. In fact, the DSC melting curves can be deconvoluted and, if we consider the endotherm area below 45 °C as the atactic content, the corresponding results for the isotactic contents are those presented in Table 1, which, considering the rather high error involved, compare well with the NMR determinations.

From these results and from the values of the molecular masses reported in Table 1, it follows that the fractionation occurs on the basis of both molecular mass and tacticity differences, with the atactic content concentrated in the lower molecular mass chains.

The DSC determination of the isotactic content has been done by assuming that the melting enthalpies of the atactic and isotactic crystals are the same. In fact, the total enthalpies of the three samples are slightly different (Table 1). From these values and the approximate isotactic contents, it can be deduced that the melting enthalpies of the purely atactic and isotactic samples are of the order of $105 \pm 10$ and $125 \pm 10$ J/g, respectively.

The WAXS patterns for the three samples are shown in Figure 5. It can be observed that whereas the soluble fraction presents a single diffraction peak, the IF sample shows several peaks, even at low angles, indicating a much higher degree of order in this sample (the pattern of the original sample is in between the two). Thus, peaks at 3.53, 1.76, 1.18, 0.50, 0.44, 0.42 and 0.375 nm are clearly observed in the IF sample, arising from the planes (020), (040), (060), (091), (171), (191) and (200), respectively, of
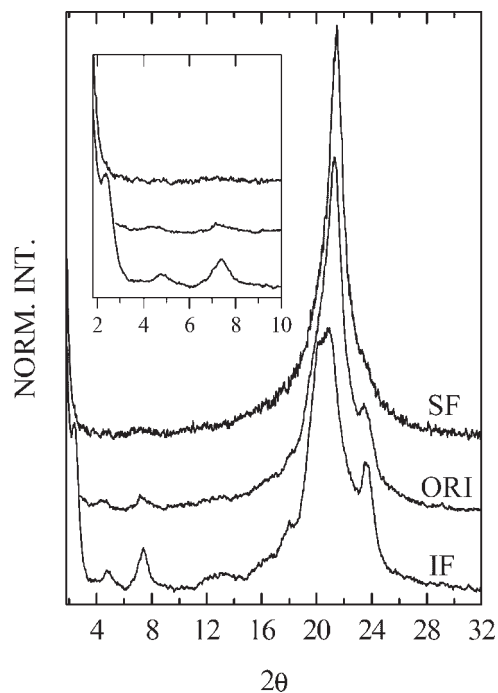


Figure 5. X-ray diffractograms of the three POD samples. From top to bottom: soluble fraction (SF), orginal sample (ORI) and insoluble fraction (IF).

the type II crystal form reported by Turner-Jones,[10] corresponding to an orthorhombic unit cell, similar to the one found in polyethylene and long-chain hydrocarbons.

Regarding the diffractogram for sample SF, a single strong peak centered at 0.415 nm is observed; no low-angle reflections are detected. These features are characteristic of parallel hydrocarbon chains arranged side-by-side in a hexagonal network, but in a random orientation or oscillating about their chain axis.[10] This low-order crystal structure is the one assumed by efficiently quenched isotactic long-chain poly($\alpha$-olefins), where the quenching process only allows a limited degree of order, with the main chains basically disordered. It is reasonable that a similar situation is present in the case of atactic chains, where the absence of stereoregularity is responsible for the lack of ordering in the main chain.

The question is whether the atactic chains can develop higher degrees of order. We plan to analyze this aspect by annealing the atactic polymer at different temperatures for different amounts of time. The molecular mass may also have some influence, so that we will study samples of different molecular mass.

In Figure 6, the CPMAS spectra of the solid SF and IF samples are shown. An obvious difference between these spectra is the distinct character of the resonances downfield from the main peak in the IF spectrum and their near absence in the SF spectrum. From Table 2, the most likely carbons associated with these downfield peaks are the $\alpha$ and 16B methylene carbons; these are carbons in or near the backbone. Since the sharpness of resonances in the solid state is generally associated with low mobility and well-defined molecular packing,[19] these results suggest that the dominant crystal structures of the SF and IF samples lack and possess backbone crystallinity, respectively. There is also a modest difference in resolution, seen most clearly in the shapes of the minor signals. Finally, the chemical shift for the main resonance of IF and SF was $33.00 \pm 0.10$ and $33.47 \pm 0.10$ ppm. For reference, at this field strength, the resonance of carbons in the orthorhombic crystalline phase of linear polyethylene appear at $33.11 \pm 0.05$ ppm.[20]

Figure 7 compares the spectra of the CR regions of the SF and IF samples. These spectra have been derived from linear combinations of CPMAS spectra with 0 and 12 ms spin locking times. The linear combinations are chosen based on elimination of the shoulder near 31 ppm, the spectral region where interior methylene carbons appear when they are in linear aliphatic chains undergoing rapid trans-gauche isomerization.[21] This method for isolating the spectrum of the CR regions, to a first approximation, preserves the relative intensities of all carbons occupying those regions. We will now discuss certain facets of the CR spectrum of the IF sample providing some insight into the molecular dynamics in the unit cell and some modest support for the X-ray structure of isotactic polyoctadecene (i-POD) proposed by Turner-Jones.[10]

In the studies of Turner-Jones on isotactic poly(1-alkenes), including i-POD, it was hypothesized, based on X-ray observations, that the most likely structure for i-POD was an orthorhombic unit cell with eight repeat units and a backbone that is a 'quaternary helix'. Whereas no specific coordinates were offered for the backbone carbons, the drawings indicated that 'quaternary helix' referred to a
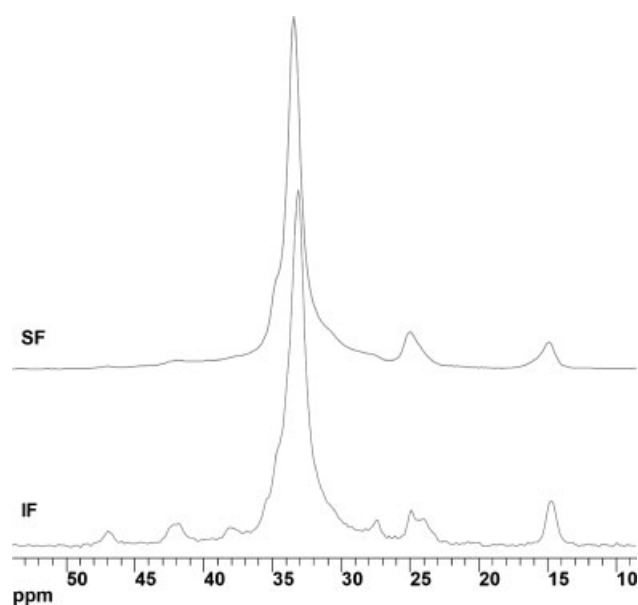


Figure 6. CPMAS $^{13}$C NMR spectra (25.2 MHz) of the insoluble fraction (IF, lower) and soluble fraction (SF, upper) of POD samples.
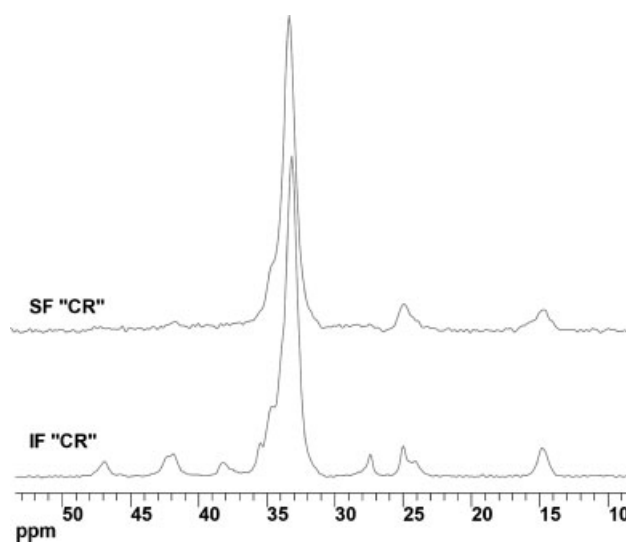


Figure 7. Comparison of lineshapes associated with the crystalline regions of the insoluble fraction (IF, lower) and soluble fraction (SF, upper) of POD samples. Sharper features in the IF spectrum indicate a higher level of order. The existence of sharper downfield features in the IF spectrum indicates backbone order; lack of such features in the SF spectrum shows backbone disorder.

backbone structure approximating a $4_1$ helix. Furthermore, the sidechains were believed crystallized in extended conformations so that the axes of the extended sidechains of a given molecule make an angle of about 130.6° with respect to the helical backbone axis. In addition, the extended portions of all sidechains of a given molecule create a herringbone pattern. Adjacent sidechains, taken pairwise, are parallel to each other, and successive pairs are positioned on opposite sides of the backbone. Finally, the proposed three-dimensional sidechain packing is like orthorhombic polyethylene (PE). It is clear that in order to enable adjacent sidechains of a given pair to extend parallel to one another, supposing that the backbone is approximately a $4_1$ helix, the detailed conformations of each chain cannot be the same, at least not in the vicinity of the backbone. Also, such a crystal structure will certainly not have a $4_1$ helical symmetry. Moreover, in order to generate a backbone with an approximate $4_1$ helix, the conformations of the backbone carbons must depart from ideal tetrahedral bond angles.[22] The solid state NMR results allow us to comment on a few of these structural claims.

The easiest issue to comment on, regarding the IF sample, is the notion that the sidechains are packed in a similar manner as that found in orthorhombic PE. We can check this using the chemical shifts of the interior methylene carbons of the sidechains. For the IF sample, this shift is $33.00 \pm 0.10$ ppm and is very close to the chemical shift, $33.11 \pm 0.05$ ppm, of orthorhombic PE.[20] This is significant in view of the fact that the methylene chemical shift shows some sensitivity to different types of crystal packing for the alkanes.[23] For example, at 2.35 T, we measure the following methylene shifts for other types of alkane crystal packing: triclinic phase in eicosane, like monoclinic PE $34.40 \pm 0.15$ ppm, and the rotator phase in nonadecane (C19), $33.45 \pm 0.08$ ppm. Thus, the shift supports a packing of sidechains similar to orthorhombic PE.

In terms of assignments, relative intensities can help us decide how many carbons are associated with each line. For the spectrum of the CR region of sample IF, the shifts (and numbers of carbons represented) are: 14.8 (1.0), 23.5–25.5 (1.0), 27.3 (0.5), 32–36 (13.5), 38.2 (0.5), 42.0 (1.0), and 46.7 ppm (0.5). It is, therefore, clear from the shifts with associated "0.5" intensities that the resonances of at least two carbons from the isotactic polyoctadecene (i-POD) repeat unit are split quite widely. The pairings for the split resonances are ambiguous, however, especially recognizing the emerging doublet character of the 42 ppm resonance. For example, the resonances on the downfield side of the main resonance (probably assigned to $\alpha$ and 16B carbons based on Table 2), might represent either a single, large 8.5 ppm splitting (38.2 and 46.7 ppm) or two splittings that are in the range from 3.5 to 5.0 ppm. It is important, in terms of the backbone conformation in the i-POD unit cell, whether there is one large splitting or two smaller ones. An 8.5 ppm splitting is certainly possible. In fact, it is close to

the splittings observed for the methylene backbone carbons in solid forms of syndiotactic polypropylene (s-PP)[24,25] and in syndiotactic poly(1-butene) (s-PB)[26] and its propene copolymers.[27] In all of these cases, the splittings are associated with a TGGT (T = trans, G = gauche) backbone conformation, and the shifts are rationalized qualitatively by the fact that consecutive backbone methylenes alternate between having $n$ or $(n-2)$ total $\gamma$-gauche interactions with other carbons. The significance of such $\gamma$-gauche interactions for determining chemical shifts has been recognized,[28] and it is expected that an upfield shift increment of about $-4$ to $-6$ ppm is associated with each additional $\gamma$-gauche interaction that the $\alpha$ carbon experiences. Thus, in order to generate a splitting as big as 8.5 ppm, a difference of two $\gamma$-gauche interactions is necessary. A TGGT backbone conformation in head-to-tail polymerized 1-alkene polymers has the property that consecutive $\alpha$ carbons alternate between having zero and two $\gamma$-gauche interactions involving backbone 'br' carbons. For i-POD, each $\alpha$ carbon has potential $\gamma$-gauche interactions not only with two 'br', but also with two 15B carbons. Thus, if the number of $\gamma$-gauche interactions with all 15B carbons were the same for each $\alpha$ carbon, one could entertain the possibility that the real splitting is 8.5 ppm *and* that the i-POD backbone conformation is TGGT. Such a conformation would be at variance with the "quaternary helical" backbone proposed by Turner-Jones. Hence, consistency with the Turner-Jones structure requires that we either eliminate the TGGT possibility or, at least, argue against its plausibility.

If we assume there is an 8.5 ppm splitting of the $\alpha$ carbon in i-POD, one argument against the plausibility of a TGGT conformation comes from the average shift difference, around $-6$ ppm, for the $\alpha$ carbons of s-PB[26,27] relative to those of i-POD. (The s-PB and i-POD polymers are similar in the important sense that the sidechains of each are sufficiently long so that both sidechain and backbone carbons can contribute to the possible $\gamma$-gauche interactions of the $\alpha$ carbons.) Such a shift difference would usually indicate that, on average, each $\alpha$ carbon in s-PB would have one more $\gamma$-gauche interaction than its counterpart in i-POD. Since the maximum number is four for both polymers, the deduction would be that the $\alpha$ carbons of i-POD would alternate between one and three $\gamma$-gauche interactions. This is impossible since every $\alpha$ carbon of i-POD must have at least two such interactions. Therefore, it is implausible that both the large splitting and the TGGT backbone are simultaneously true for i-POD.

An argument against the existence of a large splitting is a chemical shift argument. If the $\alpha$ carbon is split by 8.5 ppm, its mean shift is 42.5 ppm compared to the solution value of 40.3 ppm. Actually, this is a reasonable shift between solid and solution and is similar to that seen in linear polyethylene,[21] albeit the understanding of the sign of the shift in the latter case is that the solid state is strongly biased

towards the trans conformation compared with the solution state. Nevertheless, the main problem arises when the remaining i-POD resonance at about 42 ppm is assigned to the next most likely candidate, i.e., 16B. In that case, one would have to invoke a 7 ppm downfield shift upon going to the solid state. This magnitude of shift is highly unlikely, given that the rest of the shifts seem to lie within 3 ppm of the solution-state values. Hence, we conclude that there is a higher likelihood that both the α and 16B carbons have shifts of about +5 ppm upon going from solution to the solid state and that the splittings of the crystalline α and 15B carbons are in the range from 4.5 to 5.0 ppm. Note that the foregoing arguments have not completely eliminated the possibility that the TGGT backbone conformation exists; we are simply saying that plausibility arguments point to two smaller low-field splittings rather than one large one. Thus, if a TGGT backbone conformation exists, the number of γ-gauche interactions between α and 15B carbons will not be the same for all α carbons.

Experimentally, we performed one, rather simple test to make sure that none of the three downfield resonances was associated with the 'br' carbon. This test involved the technique of cross polarization/depolarization.[29] This experiment is performed as a CPMAS experiment, except that observation is delayed by a brief time, $\tau_{ph}$, during which the $^{13}$C rf phase is switched by 180°. This phase switch causes the signal to move towards inversion and spectra covering the range of $\tau_{ph}$ from 20 to 40 μs are shown in Figure 8. The $\tau_{ph}$ corresponding to a 'null condition' decreases for increasing numbers of protons attached to the carbon and decreases with increasing extent of motional averaging of the $^{13}$C-$^1$H dipolar interaction. Thus, for example, the fast rotation of the methyl carbon results in a sluggish nulling. For relatively rigid methylenes, signals pass through zero for $\tau_{ph} \approx 23$ μs; for methines, the same condition prevails for $\tau_{ph} \approx 35$ μs. In this way, by choosing the appropriate $\tau_{ph}$, one can suppress either the signals from the rigid methylenes, relative to the methines, or vice versa. Figure 8 shows such spectra as a function of the indicated depolarization times. A 5 ms proton spin lock has been applied prior to any cross polarization in order to enhance the ratio of crystalline to noncrystalline contributions to these spectra; such a strategy approximately cuts the noncrystalline contribution in half; however, there are still some noncrystalline contributions evident in Figure 8. The important qualitative results from Figure 8 are: a) the three downfield resonances of the IF sample retain their relative intensities; hence, all of these resonances belong to relatively rigid methylene groups; b) the main methylene peak does not behave uniformly, i.e., the downfield side passes through the null more slowly than the upfield side, but not as slowly as the wide upfield wing in the 30 to 32 ppm region. Thus, the latter wing represents the most mobile carbons, which are mainly noncrystalline carbons; c) the most downfield shoulder of the main line at 35.5 ppm can be assigned to the 'br'



Figure 8. Distinguishing of rigid methylene and methine signals using polarization/depolarization spectra for the insoluble fraction (IF). After 5 ms of spin locking followed by 1 ms of cross polarization, there is a 180° phase shift of the carbon rf for a duration of $\tau_{ph}$. Spectra from top to bottom have $\tau_{ph} = 20, 23.2, 26.5, 30, 34$ and 40 μs. Relatively rigid methylene carbons null near 23 μs, whereas methine carbons null near 35 μs. Motional averaging, e.g. for methyls near 15 ppm, increases the time needed for nulling.

carbon. The narrow character of this line, as revealed in Figure 8, along with the relative intensity indicated in Figure 7, combine to suggest that this is also a split resonance. In view of the inhomogeneous behavior of the main peak, the counterpart 'br' resonance cannot be determined unambiguously from Figure 8; however, indications are strongest at 34.0 ppm.

As an aside, the 2B resonance in Figure 7 has a broad upfield wing along with a sharper downfield feature. The behavior of this methylene intensity in Figure 8 shows that the broad upfield wing is associated with more motional averaging than is the downfield feature; however, there is also some motional averaging of the sharper feature because it nulls near 28 μs, i.e., quite a bit later than the other, more rigid methylene resonances. In any case, there is a substantial qualitative difference between the packing constraints for 2B within the CR region.

The splittings identified for the α, br, and 16B carbons are all consistent with the coexistence, within the unit cell, of branching geometries that are inequivalent. In this limited

sense, the Turner-Jones structure is supported since the conformations of consecutive chains in their structure cannot be the same. It is logical to expect that the impact of this dissimilarity would extend to the backbone carbons. In view of the need for succeeding chains to adopt different conformations, it is also probable that the backbone carbons will not adopt, but only approximate, a regular $4_1$ helical conformation.

There is also the issue of the second split resonance in the spectrum of the CR i-POD. The identifiable resonance is at 27.5 ppm, and the other half of that resonance is underneath the main line from 32 to 36 ppm. Thus, the center of mass of the doublet lies in the range from 29.8 to 31.8 ppm. In view of the foregoing discussion and the data of Table 2, the assignment of the 27.5 ppm resonance likely involves one of the carbons in the group from 3B to 14B. We would surmise that this assignment would pertain to a carbon closer to the point of attachment, i.e., 13B or 14B.

It is interesting that the 2B resonance of the CR IF region in Figure 7 shows two features, namely, a) a total relative integral that is very close to 0.055, the theoretical value for representation of a single carbon and b) a line with a distinct upfield shoulder. The latter may indicate that near the ends of the sidechains, packing is not always ideal in the CR regions, or this may be an outgrowth of the fact that the two consecutive parallel sidechains are not in registry according to their lengths. From the diagrams of Turner-Jones, it is not clear whether the end groups are expected to pack in good registry. The mobility differences between the wing and sharper feature of this resonance are not only visible in the polarization/depolarization spectra of Figure 8; differences are also detected in the longitudinal $^{13}$C relaxation time, $T_1^C$. The higher mobility of the upfield wing of this line is reflected in a $T_1^C$ of $0.9 \pm 0.3$ s, whereas the $T_1^C$ of the main, downfield resonance is about $7 \pm 2$ s. Moreover, the average 2B mobility is significantly greater than for most of the interior methylene carbons, both backbone and sidechain, whose average $T_1^C$'s are $30 \pm 10$ s. An exception to the latter characterization is the $T_1^C$ ($6 \pm 2$ s) of the upfield portion of the doublet at 42 ppm. Thus, among the downfield resonances (38.2, 41.8, 42.2 and 46.7 ppm), whose splittings were discussed, the 41.8 ppm resonance shows a modestly higher mobility as reflected in the $T_1^C$ behavior, whereas differences in the average strength of the $^{13}$C-$^1$H dipolar couplings are very minor for each of these resonances, as seen from the similarity of the response in the polarization/depolarization spectra of Figure 8. Thus, contrasting mobility, as seen via $T_1^C$, is observed within the 2B lineshape and within the 42 ppm doublet. However, this mobility difference is not evident in the polarization/depolarization spectra for the 42 ppm doublet, yet it is very evident for the 2B resonance. A likely explanation for this contrasting behavior is that the mobile wing of 2B represents highly mobile chain terminae whose correlation times, according to the measured[30] $T_1^C$, are in the $10^{-10}$ to $10^{-11}$ s

range, whereas $T_1^C$'s for the other three resonances suggest correlation times in the $10^{-5}$ to $10^{-6}$ s range where averaging of the $^{13}$C-$^1$H dipolar interactions is not nearly as efficient.

Finally, we say a word about the contrast in mobility for the crystalline chains in the SF and IF samples. Respective $T_1^C$'s are $0.7 \pm 0.2$ and $30 \pm 10$ s implying that there is considerably more mobility in the SF crystalline regions. We also looked for evidence of contrasting mobilities in the proton rotating frame relaxation time, $T_{1\rho}^H$. However, contrast in $T_{1\rho}^H$, as monitored via the main CR peaks, was only modest. $T_{1\rho}^H$'s were $27 \pm 3$ and $36 \pm 3$ ms for the SF and IF samples, respectively. Thus, the mobility contrast between these samples shows up more clearly at mid-MHz frequencies (via $T_1^C$) than at mid-kHz frequencies (via $T_{1\rho}^H$). This may, in part, be due to the influence of proton spin diffusion which can cause $T_{1\rho}^H$ measurements of CR spectral features to be influenced by $T_{1\rho}^H$ relaxation in noncrystalline regions. Spin diffusion plays a much smaller role in $T_1^C$ measurements; thus, the contrast in $T_1^C$ for the CR carbons of the SF and IF samples truly reflects substantial differences in mid-MHz motions. The $T_1^C$ of 0.7 s for the SF sample is of the same order as that of the rotator phase of C19, $1.7 \pm 0.1$ s. There is also a parallel similarity of chemical shift, $33.47 \pm 0.10$ ppm for crystalline SF and $33.45 \pm 0.08$ ppm for C19. Thus, there is a modest support for the idea that the sidechain crystallinity of the SF sample results in a sidechain organization where there is substantial motion around the sidechain axes. This would be consistent with the lower melting point and smaller heat of fusion of the SF versus the IF samples.

## Conclusions

The results show that the fractionation of the original poly(1-octadecene) sample, synthesized with a highly active heterogeneous Ziegler-Natta catalyst, occurs on the basis of both molecular mass and tacticity differences, with the atactic content concentrated in the lower molecular mass chains. Thus, the soluble fraction, having a lower average molecular mass than the original sample, consists predominantly of atactic chains, whereas the insoluble fraction is mainly isotactic. The analysis of the solid-state structure reveals that both atactic and isotactic fractions are able to crystallize, although the resulting structures are different. The NMR and WAXS data together support the "most probable" structure for the isotactic polymer advanced by Turner-Jones, namely, an orthorhombic crystal form, where the sidechains pack in a way analogous to orthorhombic polyethylene and where successive sidechains on a given molecule exhibit different conformations in the vicinity of the backbone. The backbone crystallizes; however, we are unable to verify that the backbone conformation is as proposed, i.e., close to a $4_1$ helical conformation (as opposed to, say, a TGGT conformation). On the other

hand, the crystal form for the atactic polymer shows only sidechain order with some support for the notion that this order approximates the disordered hexagonal rotator phase of the alkanes.

[1] N. A. Platé, U. P. Shibaev, ''*Comb-shaped Polymers and Liquid Crystal*'', J. M. G. Cowie, Ed., Plenum Press, New York 1987.
[2] P. L. Magagnini, *Makromol. Chem.* **1981**, 223.
[3] J. Wang, R. S. Porter, J. R. Knox, *Polymer J.* **1978**, *6*, 619.
[4] K. Soga, D. H. Lee, T. Shiono, *Makromol. Chem.* **1989**, *190*, 2683.
[5] B. Peña, J. A. Delgado, A. Bello, E. Pérez, *Makromol. Chem., Rapid Commun.* **1991**, *12*, 353.
[6] B. Peña, J. A. Delgado, E. Pérez, A. Bello, *Makromol. Chem., Rapid Commun.* **1992**, *13*, 447.
[7] D. W. Aubrey, A. Barnatt, *J. Polym. Sci., Part A: Polym. Chem.* **1968**, *6*, 241.
[8] A. L. Segre, F. Andruzzi, D. Lupinacci, P. L. Magagnini, *Macromolecules* **1981**, *14*, 1845.
[9] J. J. Mallon, S. W. Kantor, *Macromolecules* **1989**, *22*, 2077.

[10] A. Turner-Jones, *Makromol. Chem.* **1964**, *71*, 1.
[11] M. Peeters, B. Goderis, C. Vonk, H. Reynaers, V. Mathot, *J. Polym. Sci., Part B: Polym. Phys.* **1997**, *35*, 2689.
[12] T. G. Scholte, N. L. J. Meijerink, H. M. Schoffeleers, A. M. G. Brands, *J. Appl. Polym. Sci.* **1984**, *29*, 3763.
[13] J. Schaefer, E. O. Stejskal, R. Buchdahl, *Macromolecules* **1975**, *8*, 291.
[14] D. L. VanderHart, E. Pérez, *Macromolecules* **1986**, *19*, 1902.
[15] D. A. Torchia, *J. Magn. Reson.* **1978**, *30*, 613.
[16] W. E. Earl, D. L. VanderHart, *J. Magn. Reson.* **1982**, *48*, 35.
[17] J. C. Randall, in: *Polymer Characterization by ESR and NMR*, ACS Symp. Ser. 142; A. E. Woodward, F. A. Bovey, Eds., American Chemical Society, Washington, DC 1980.
[18] L. P. Lindeman, J. Q. Adams, *Anal. Chem.* **1971**, *43*, 1245.
[19] D. L. VanderHart, W. L. Earl, A. N. Garroway, *J. Magn. Reson.* **1981**, *44*, 361.
[20] D. L. VanderHart, *J. Chem. Phys.* **1986**, *84*, 1196.
[21] W. E. Earl, D. L. VanderHart, *Macromolecules* **1979**, *12*, 762.
[22] L. A. Belfiore, F. C. Schilling, A. E. Tonelli, A. J. Lovinger, F. A. Bovey, *Macromolecules* **1984**, *17*, 2561.
[23] D. L. VanderHart, *J. Magn. Reson.* **1981**, *44*, 117.
[24] A. Bunn, M. E. A. Cudby, R. K. Harris, K. J. Packer, B. J. Say, *J. Chem. Soc., Chem. Comm.* **1981**, 15.
[25] P. Sozzani, R. Simonutti, M. Galimberti, *Macromolecules* **1993**, *26*, 5782.
[26] C. De Rosa, G. Guerra, A. Grassi, *Macromolecules* **1996**, *29*, 471.
[27] C. De Rosa, F. Auriemma, D. Capitani, L. Caporaso, G. Talarico, *Polymer* **2000**, *41*, 2141.
[28] A. E. Tonelli, *Macromolecules* **1978**, *11*, 565; Ibid. p. 634.
[29] X. Wu, K. W. Zilm, *J. Magn. Reson., Ser. A*, **1993**, *102*, 205.
[30] A. Abragam, ''*The Principles of Nuclear Magnetism*'', Oxford University Press, London 1961, Chap. 8.